Tropical instability waves in the Atlantic ocean: a contributor to biological processes

Long instability waves
Oceanic general circulation model
Biological production
Intertropical Atlantic

Ondes longues d'instabilité
Modèle de circulation générale océanique
Production biologique
Atlantique intertropical

Alain MORLIERE [a*], Aubert LE BOUTEILLER [b] and Jean CITEAU [c]

[a] Laboratoire d'Océanologie Dynamique et de Climatologie,
Unité Mixte CNRS/ORSTOM/Université Paris 6, Paris, France.
[b] ORSTOM, Nouméa, New Caledonia.
[c] Unité Traitement Image Satellite, Centre Recherches Océanographiques,
Dakar, Sénégal.
* Present address: ORSTOM, 15 BP 917, Abidjan 15, Ivory Coast.

Received 23/5/94, in revised form 25/10/94, accepted 8/11/94.

ABSTRACT

Long tropical instability waves are described at around 3-4°N based on results of a simulation performed with a general circulation model for the Atlantic Ocean. This description is in agreement with earlier observations of organized undulations of the summer thermal front associated with anti-cyclonic eddies propagating westward at 30-40 km/day along 3-4°N from 10 to 40°W through the Atlantic basin. However, the simulation indicated the presence of long waves in early boreal winter. In this respect, satellite observations during short cold events in winter show thermal front undulations similar to those associated with long wave propagations.

The simulation clearly demonstrated large vertical movements between the surface and a depth of 70 m, associated with anti-cyclonic eddies at around 3°N. These vertical movements could commonly reach the thermocline in the central part of the Atlantic basin (10-20°W). In this region, long instability waves could subsequently affect biological production by "eddy pumping". During the PIRAL cruise at 4°N-20°W in June 1986, remarkably high chlorophyll concentrations (the highest values in our data bank for the equatorial Atlantic and typical of a very productive zone) were associated with currents similar to those of an anti-cyclonic eddy and characterized by a surface temperature distribution typical of the long instability wave pattern. These high chlorophyll concentrations may have resulted from "eddy pumping" and/or strong meridian advection since each of these mechanisms is associated with long instability waves.

RÉSUMÉ

Ondes tropicales d'instabilité dans l'océan Atlantique: une contribution aux processus biologiques.

Les résultats d'une simulation à l'aide d'un modèle de circulation générale sont utilisés pour décrire les ondes longues d'instabilité se propageant au voisinage de 3-4°N dans l'océan Atlantique. Ces ondes d'instabilité se caractérisent par des ondulations organisées du front thermique de surface qui existe en été boréal dans cette région. A ces ondulations sont associés des tourbillons anti-cycloniques se propageant vers l'ouest à 30-40 km/jour le long de 3-4°N à travers tout le bassin Atlantique de 10 à 40°W. Les résultats de la simulation sont en accord avec les observations antérieures.

En relation avec ces propagations autour de 3°N, la simulation montre clairement d'importants mouvements verticaux entre la surface et 70 m, associés aux tour-

billons anti-cycloniques. Dans la partie centrale de l'océan Atlantique (10-20°W) l'amplitude de ces mouvements verticaux est suffisante pour atteindre la thermocline. Les ondes d'instabilité peuvent ainsi avoir une incidence sur la production biologique dans cette région. Fortuitement, pendant la campagne PIRAL en juin 1986 à 4°N-20°W, de très fortes concentrations en chlorophylle ont été observées. Ces valeurs sont les plus fortes au sein de notre banque de données de l'Atlantique équatorial et elles sont représentatives d'une région très productive. Elles étaient associées à des courants semblables à ceux d'un tourbillon anti-cyclonique et à une distribution spatiale de la température de surface typique des structures spatiales liées aux ondes d'instabilité. Ces fortes concentrations de chlorophylle peuvent donc être associées aux ondes longues d'instabilité comme résultat de mouvement verticaux importants et/ou d'intenses transports méridiens depuis la zone productive strictement équatoriale: ces deux mécanismes sont liés à la propagation des ondes d'instabilité.

Oceanologica acta, 1994, **17**, 6, 585-596.

INTRODUCTION

In the tropical Atlantic, a thermal front separates cold water near the equator from warmer water to the north. This front exists from June through September in the climatology of sea surface temperatures (SST). During June 1983, satellite infrared SST images clearly showed its location as well as undulations from 5°E to 25°W between 1°N and 4°N (pictured on the cover of Geophysical Research Letters, special SEQUAL/FOCAL edition, August 1984). During June and July 1983, Legeckis and Reverdin (1987) monitored low-frequency westward-propagating long waves, using satellite infrared images to show meridian displacement of the front. At the same time, McPhaden *et al.* (1984) determined that the front was distorted by a series of westward-propagating cusps and troughs, similar to the long waves already observed in the Pacific (Legeckis, 1977; Legeckis and Pichel, 1984; Hansen and Paul, 1984).

Measurements with a variety of instruments have determined the main properties of these long waves. Düing *et al.* (1975) were the first to suggest a relation between Equatorial Undercurrent oscillations and instability waves resulting from horizontal shears between equatorial currents. McPhaden *et al.* (1984) found that variations of velocity, salinity and temperature with depth were associated with surface front oscillations. During June and July 1983, Weisberg (1984) used current meters moored at 15°W and 28°W to demonstrate large oscillations in the meridional current component between the surface and a depth of 60 metres. Using satellite data from 1984 to 1990 for the Atlantic, Steger and Carton (1991) gave a complete description of the long instability wave visible at the sea surface, noting the existence of an inter-annual signal in long wave activities (with a minimum in 1987) as well as large anti-cyclonic eddies associated with the crests on front undulations. Malardé *et al.* (1987), Périgaud (1990) and Musman (1992) used the altimetric signal from SEASAT or GEOSAT to describe certain characteristics of these waves.

Theoretical studies confirmed that these waves result partly from latitudinal shear between equatorial zonal currents, particularly between the South Equatorial Current (SEC) and the North Equatorial Countercurrent (NECC) (Philander, 1978; Cox, 1980), and long instability waves were clearly reproduced in a general circulation model of the Pacific and Atlantic Oceans. Seasonal changes in latitudinal shear between currents affect the amplitude, period and length of the waves, depending on the intensity of the shear. The shear also changes with longitude, affecting waves that are nonstationary in time and inhomogeneous in space. Philander *et al.* (1986) used simulation to show intense downwelling in the "cold" crests of these waves and upwelling in the "warm" troughs, with a vertical velocity between + 3.5 m/day and - 3.5 m/day at a depth of 60 m. Such variations are comparable to the mean vertical velocity component in the central equatorial Pacific.

In this study, we examined the possible biological impact of long instability waves in the equatorial Atlantic, using results from a simulation based on an ocean general circulation model (OGCM) and some observations at sea to suggest that vertical movements associated with instability waves are at the origin of a productive mechanism. In successive sections, we describe the simulation performed, the satellite data used and the main properties of long waves in the simulation, and provide illustrations of the possible effects of instability waves on biological production.

The simulation

A simulation of events in the tropical Atlantic Ocean from 1982 to 1990 was conducted using the OGCM developed at the LODYC (Laboratoire d'Océanologie Dynamique et de Climatologie) forced by observed winds. The results of this simulation provided the data used here to study instability waves and their possible impact on biological processes.

The LODYC OGCM, developed by P. Delecluse and collaborators, has already been used for different applications (Chartier, 1985; Morlière *et al.*, 1989 *a* and *b;* Madec *et al.*, 1991; Reverdin *et al.*, 1991). It solves the primary equations in the Boussinesq approximation, assuming hydrostatic equilibrium and a rigid lid. The model grid is variable. For the region considered here, the mesh size varies in latitude from 35 to 75 km and in longitude from

70 to 100 km (the scale of the eddies associated with long instability waves being around 300 km in latitude and 900 km in longitude). This version of the code stretches from one coast of the Atlantic to the other, between 30°S and 50°N, which are closed boundaries. Further details on the model version are given in Reverdin *et al.* (1991). The wind field, used to force the model, was based on merchant ship observations. Analysis by Servain *et al.* (1987) showed pseudo-stress monthly fields between 30°S and 30°N east of 60°W. Outside this zone we used the climatological wind data of Hellerman and Rosenstein (1983). Linear interpolation ensured the relation between both sets of wind data. Wind stress was calculated using the Large and Pond (1981) formulation for the drag coefficient, assuming an air-sea temperature difference of 1 °C and a relative humidity of 80%. Initially, the ocean was considered to be at rest, with temperature and salinity based on the climatology data of Levitus (1982). The model was first forced during one year with an annual mean wind (calculated on the 1982-1984 period), then during two years with a monthly mean wind. The simulation was continued thereafter using monthly wind from January 1982 to December 1990. Temperature, salinity and current fields were recorded every five days. The simulation during this 9-year period provided the model data considered here.

Satellite data

We used data from the infrared radiometer on board the METEOSAT geostationary satellite, as preprocessed by the European Space Agency. On this platform, the radiometer has only one infrared channel (from 10 to 12 mm), with a ground resolution of 5 × 5 km and a radiometric resolution of 0.5 °C, so that SST cannot be retrieved using data exclusively from METEOSAT. Nevertheless we considered the radiometric temperatures to be a qualitative representation of SST. The main difficulty in using satellite data on oceanic equatorial areas is to overcome cloud coverage. With an earth scan every 30 minutes, METEOSAT, despite lower resolution, offers a better opportunity to eliminate cloud cover than do polar satellites whose repetitivity in the equatorial region is 6 hours with a pair of satellites.

We calibrated the data by using a cold body (space) and an on-board hot body. A composite image was then obtained on the assumption that the radiometric temperature of any cloud (even in lower layers) or semi-transparent haze is less than that of the sea. Based on frequent observation of the same geographical spot (up to 48 times per day), the highest radiometric temperature value of the series of observations was presumed to have the greatest probability of being a cloud-free observation. Thus, for each pixel of a METEOSAT image, we retained (without atmospheric correction) the highest value observed among 24 images in a day. The resulting composite images used here are a qualitative representation of SST for areas that were cloud-free once a day. Geographic correction provided the usual coordinates in latitude and longitude.

Equatorial long waves: simulation and observations

Our study concerned mainly the region between the equator and 7°N and between the Greenwich meridian and 40°W, where instability waves are most visible due to the thermal surface front in summer. In this region, the main currents are zonal and subject to important seasonal variations. The westward-flowing SEC and the eastward-flowing NECC and Guinea Current are weakest during the northern spring and more intense during the northern summer and autumn. The NECC disappears at the surface in early boreal spring (Richardson and McKee, 1984). The latitudinal shear between these two currents accounts for long instability waves (Philander, 1978; Cox, 1980), the separation between the currents being around 3°N in the central part of the Atlantic.

Surface temperatures, surface currents and eddies

The oscillations of the surface thermal front around 3°N are well depicted by the simulation data during boreal summer (Fig. 1). The wavelength of these westward-propagating undulations is approximately 900 km, with a phase speed of around 30 cm/s westward (Fig. 2). These values are similar to results from observations (Legeckis and Reverdin, 1987; Steger and Carton, 1991) and from another simulation (Philander *et al.*, 1986). During the rest of the year, the thermal front does not exist normally, so that there is no possibility of instability waves appearing in the surface temperature field. However, some observations presented further in the text indicate the existence of a thermal front in boreal winter during short cold events.

The eastward flow in the North and the westward flow in the South are separated by well-formed anti-cyclonic eddies at around 3°N. These eddies are associated with the thermal front and move westward with the phase speed of the undulations of the front (Fig. 2). Such eddies have already been observed with surface drifters by Hansen and Paul (1984) in the Pacific and by Richardson and Reverdin (1987, their Fig. 21) in the Atlantic and have been determined with satellite data by Steger and Carton (1991) in the Atlantic.

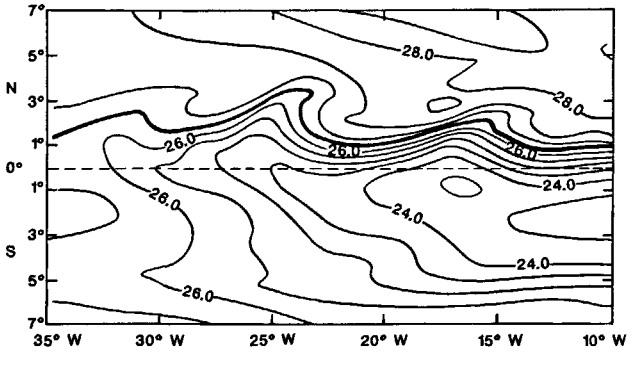

Figure 1

Sea surface temperatures simulated by the LODYC OCGM in July 1990. The equatorial SST front is outlined by the 26.5°C isotherm (thick line).

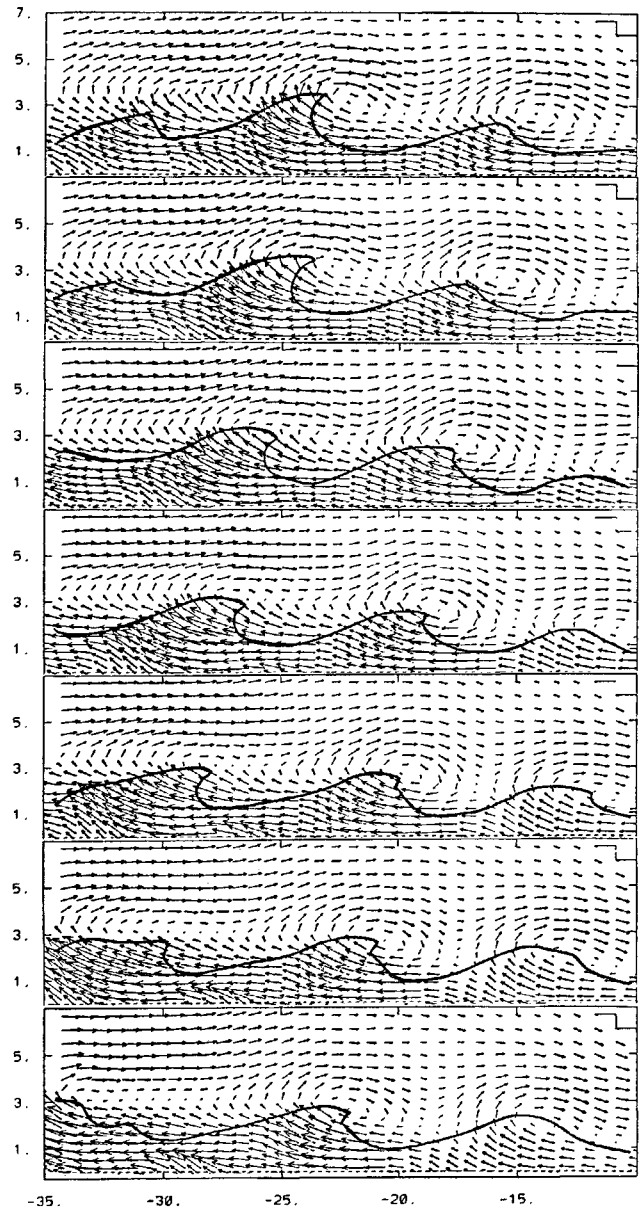

Figure 2

Time changes for the equatorial SST front (26.5 °C isotherm) and surface currents are indicated between the equator and 7°N and between 10°W and 35°W every 5 days from 5 July (top panel) to 4 August 1990.

Westward flow is intensified in the southwestern part of the eddies where water is upwelled. Northward flow is most intense on the west side of the eddies where downwelling occurs near the crest of undulations (Fig. 3).

Subsurface structures

The simulation revealed large vertical movements associated with anti-cyclonic eddies. At 50 m in depth (Fig. 4), there were positive and negative vertical velocity cores in which the vertical speed was greater than 3.5 m/day upward or downward (locally the vertical speed reached ±10 m/day). Such vertical speeds are comparable to simulated equatorial upwelling velocity, *i.e.*, around 2 m/day during boreal summer. The horizontal extension of those

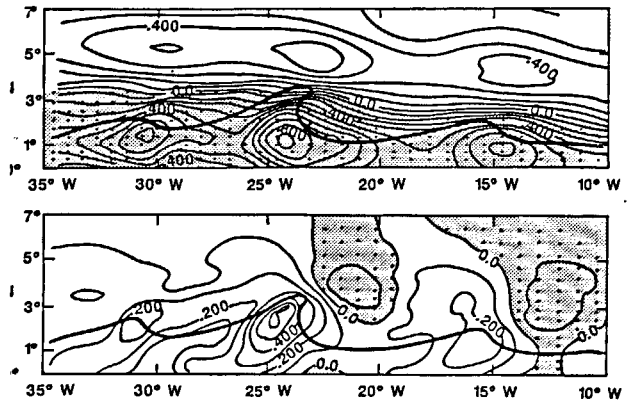

Figure 3

Simulated current for 5 July 1990: a) eastward component; b) northward component. Negative values are shaded. The heavy line represents the SST front (26.5 °C isotherm).

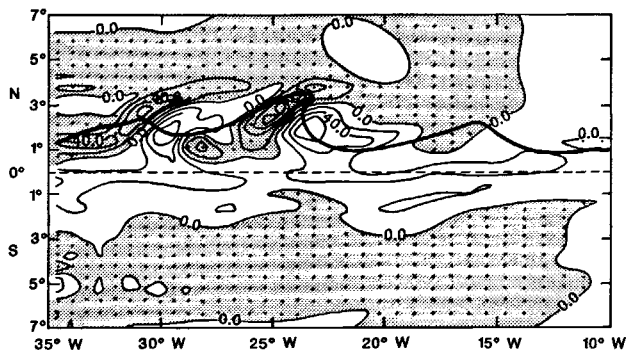

Figure 4

Horizontal distribution of the simulated vertical current component for 5 July 1990. Negative values are shaded. Velocity values in m/s are multiplied by 10^6. The heavy line represents the SST front (26.5 °C isotherm).

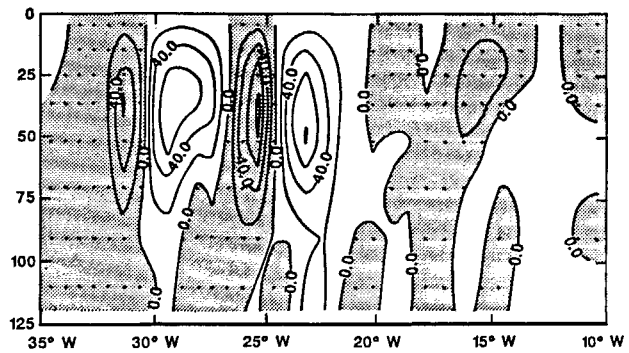

Figure 5

Vertical distribution of simulated vertical velocity along 2°N for 5 July 1990. Negative values are shaded. Velocity values in m/s are multiplied by 10^6.

regions of high vertical velocity is roughly 300 km, and the vertical extension is from the surface to 80 m in depth near 2°N (Fig. 5). The vertical temperature section at 2°N displays vertical chimneys of cooler water (Fig. 6). If the chimneys do not coincide with the upward velocity zones on Figure 5, this is not because of different dates. The

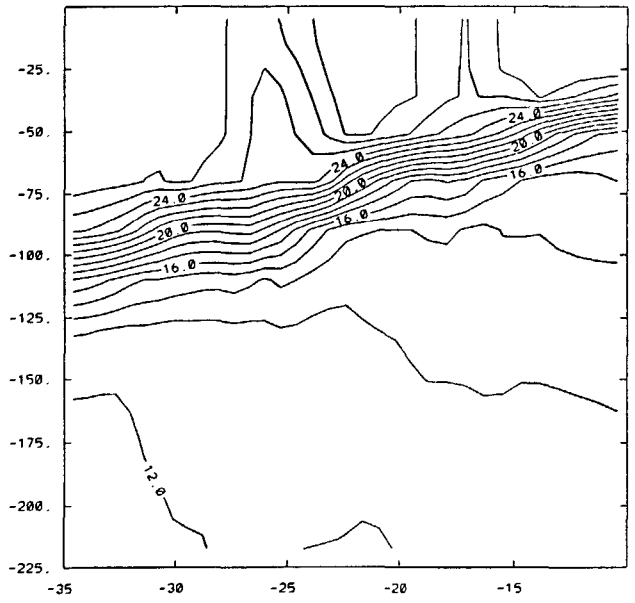

Figure 6

Vertical distribution of simulated temperature along 2°N for 10 July 1990.

coolest temperature is always located on the chimney centre between the upward and of downward velocity zones, a feature characteristic of the instabilities. This can be explained simply by considering a water parcel crossing first an upward velocity area then a downward velocity area with a much greater horizontal than vertical velocity. The trajectory summit is reached when the vertical velocity is null, and the temperature is minimal at that point.

Seasonal variations

Long instability waves do not exist throughout the year. Satellite observations (Steger and Carton, 1991) indicate that long wave activity begins in June and persists through mid-September. Nevertheless, the westward-propagating waves last until the end of the year in model simulation. From 2 to 4 long instability waves cross the basin each summer from 10 to 40°W, and several weaker waves propagate mainly west of 20°W from October to January. During boreal summer, the long waves propagate more rapidly (20-42 cm/s) than during the period from October to January (17-30 cm/s). Legeckis (1986), using satellite data, observed a decrease of phase speed before the end of the summer wave events (from 48 cm/s in June to 20 cm/s in August 1983). No long waves were included in the simulation during March-April when latitudinal current shear ceases with the disappearance of the NECC during the northern spring (Fig. 7).

As the thermal front is normally present only from June to September, it is not possible to visualize long waves by thermal satellite observations during part of the year. However, some observations from the METEOSAT satellite show sea surface coolings during boreal winter in the equatorial zone. At that time, the Intertropical Convergence Zone (ITCZ) moves towards its most southern latitude and the equatorial zone is more cloudy. Such cold events were observed between 3°N-3°S and 5°W-25°W in January 1986, December 1989 and January 1990. During these events, there was a well-developed thermal front, with a temperature gradient of 1.5 °C in 1986 and 2.5 °C in 1989 and 1990. The undulations of the front were similar to those observed during summer, confirming the existence of long waves in winter as suggested by model simulation (Fig. 8). *In situ* observations of such cold events at the equator during the northern winter are quite rare but were noted before (probably for the first time) by Molinari *et al.* (1983) using the First GARP Global Experiment (FGGE) observations in the equatorial Atlantic. The predominant feature of surface temperature distribution in January-February 1979 during FGGE was an enclosed patch of colder water centred somewhat south of the equator at about 16°W. The SST was less than 26.2 °C at the equator within the patch but greater than 28.5 °C to the east and 27.2 °C to the west of the patch (see Fig. 1 in Molinari *et al.*, 1983).

Inter-annual variations

In the simulation, long instability waves appeared every year during the summer between 1982 and 1990, but the wave activity was weak in 1983, 1984, 1990 and strong in 1986 (Fig. 7). Wave activity was strongly reduced in 1984 in our simulation, probably in association with the "1984 Atlantic event" occurring one year after the 1982-83 Pacific El Niño (Hisard *et al.*, 1986). Pullen *et al.* (1987) noted that long waves were absent in the Pacific during the El Niño years. Steger and Carton (1991) pointed to 1987 as the most atypical year (weakest wave activity) between 1984 and 1990, although the summer of that year was not so atypical in our simulation.

PIRAL cruise results

The PIRAL cruise was carried out on board *R.V. Le Noroît* in the northeastern tropical Atlantic from the end of June to early August 1986. The cruise was divided into three periods of observations: the first (12 days) in the north equatorial convergence zone (4-6°N, 17-20°W), and the second (8 days) and third (10 days) in the Guinea Dome area, at the centre of the dome and at a short distance from it (Oudot, 1989). Our interest here concerns the first part of the cruise in the north equatorial convergence.

Physical field observations

During the first 7 days of PIRAL, the vessel followed a surface buoy fitted to a drifting *in situ* double primary production line (a set of bottles of 300 ml to 2 litre capacity between the surface and 120 m depth). This line drifted during several days in an anti-cyclonic eddy similar to those described by observations (Richardson and Reverdin, 1987) and given by model simulation.

The coupled production lines were deployed at 4°N, 20°W, on 22 June 1986 (day 1). At the end of day 3, the lines were set up on board, and the ship sailed overnight toward the starting position. Thus, on day 4, the experiment restar-

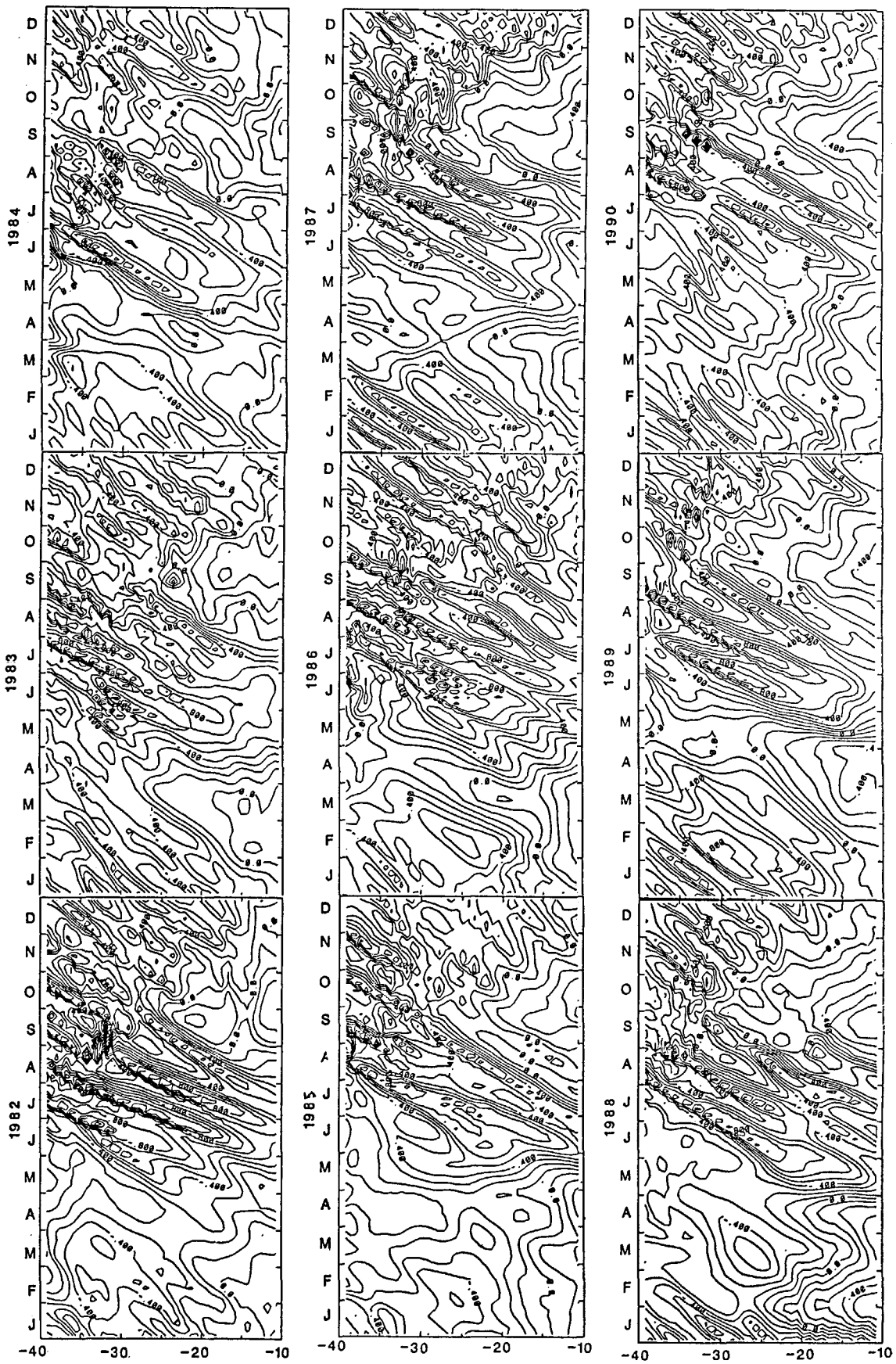

Figure 7

Times series for simulated northward velocity between 10°W to 40°W along 2°N from 1986 to 1989.

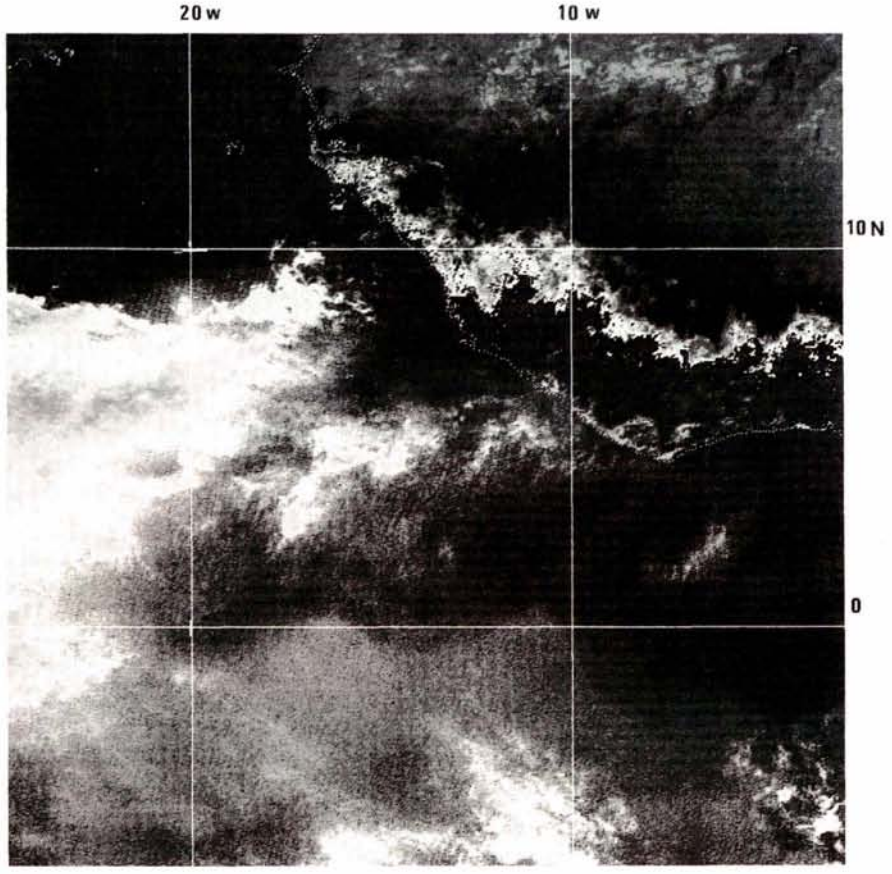

Figure 8

Radiometric temperature distribution for 26 December 1989 (composite of 24 infrared scans by METEOSAT satellite).

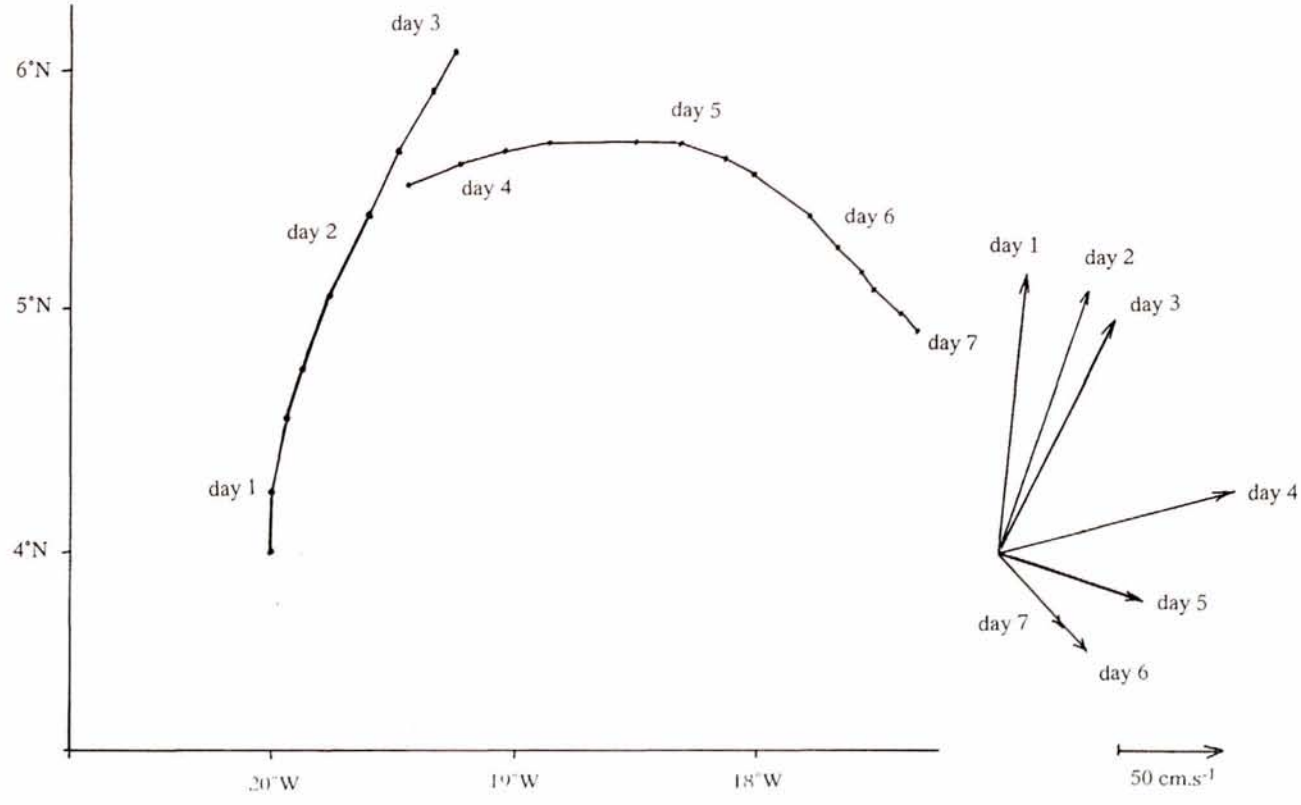

Figure 9

Drifting buoy trajectories and mean daily currents for 7 days during the PIRAL cruise in June 1986. Drift is representative of the current measured at 30 m.

Table 1

		day 1	day 2	day 3	day 4	day 5	day 6	day 7
Drifting buoy	Direction	10°	25°	30°	70°	100°	135°	140°
	Speed	140	140	130	120	110	90	50
Current (30m) at 7.00 am	Direction	no data	no data	no data	65° 130	90° 80	155° 120	155° 50
Current (30m) at 6.00 pm	Direction	no data	no data	no data	75° 110	110° 100	170° 90	180° 65

ted at the position 5°30 N, 19°30 W. From day 8 to 12, the lines were set on board every night, and the ship sailed overnight toward the initial position of day 1, *i.e.*, 4°N, 20°W. Thus, during that time, the drifting data concerned only a part of a day. The wind blew from the south on day 1 (5 to 7 m/s), weakening from day 2 to day 6 (2 to 5 m/s), and then blew from south to southeast from day 7 to day 12 (5 to 10 m/s).

The *in situ* primary production lines drifted northward on day 1 (Fig. 9) at 140 cm/s, then turned progressively northeastward during the following days. The drift became eastward with a speed of 100 cm/s on day 5 and then weakened with a southeastward direction during subsequent days (Tab. 1). After day 7, the upper layer current flowed to the southeast at about 50 cm/s. Two current profile measurements per day, at 7.00 a.m. and 6.00 p.m., showed that the drift of the lines was representative of the current measured at 30 m (Tab. 1). The strong current layer was about 40 m thick (Fig. 10).

The temperature time series indicated a slight increase of surface temperature from 26.2 °C to 27 °C, and a thermocline depth from 60 to 80 m (Fig. 11a). Salinity was minimal at the surface and maximal between 50 and 100 m (35.8 to 36.0 psu) (Fig. 11b). Nutrients, especially nitrates (Fig. 11c), were rather constant during the part of the cruise considered here. The top of the nitracline, defined as the depth of layer $[NO_3]$ = 0.1 mmole/kg, ranged from 50 to 85 m (mean 59 m). The sharp nitracline was directly related to the thermocline and extended from 60 to 90 m. More than 20 mmoles/kg of NO_3 were observed below 100 m.

Schematically, the hydrological structures during the PIRAL cruise were not very different from those observed along 5 sections at 23°W during the FOCAL programme from July 1982 to July 1984 (Oudot, 1987), except for the surface currents represented here by the drift of the *in situ* primary production line. This line drifted during several days as it was in an anti-cyclonic eddy similar to those already described by early observations and given by the model simulation (Fig. 2).

Satellite data during PIRAL

From METEOSAT infrared data, it is clearly evident that long instability waves were present and active during the PIRAL cruise. Unfortunately, the cloud cover did not allow us to obtain sea surface radiances during the first part of the cruise (22-27 June 1986), the best image being obtained for 29 June (Fig. 12). Thus, the surface currents observed during the cruise are coherent with the anti-cyclonic circulation revealed by the thermal structures in

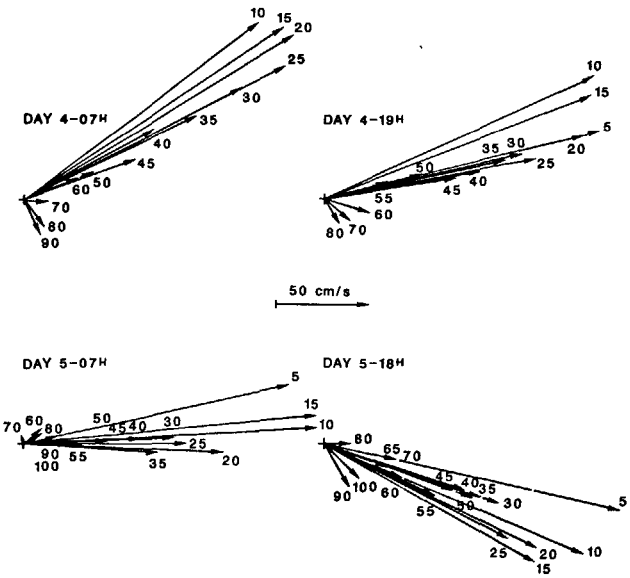

Figure 10

Currents observed for day 4 and 5 of the PIRAL cruise between the surface and 100 m in depth using a current profiler.

satellite imaging. These conditions are typical of long instability waves.

Chlorophyll and primary production observations

The vertical distribution of phytoplankton was described by 4 samplings per day. A deep chlorophyll maximum (DCM) was observed systematically between 40 and 60 m depth, just at the top of the nitracline where NO_3 was always 0.1–0.2 mmol/m³. These properties suggest that the system may be defined as a Typical Tropical Structure (TTS) such as described by Herbland and Voituriez (1979). In the TTS, the mean chlorophyll concentration in the DCM is inversely related to its depth (Fig. 14).

During our study, the DCM showed a surprisingly great variability between samplings (Fig. 13). On several occasions during the first five days, the chlorophyll concentrations reached values exceeding 1 mg/m³. Variations in the nitracline depth were too small to account for such large changes in the DCM concentration. The highest chlorophyll abundances, which indicate a major enrichment process, occurred when the current in the upper layer presented a positive northward component. After day 5, the current was still rapid in the surface layer (150 cm/s at 15 m depth on day 6 at 7.00 a.m.), but the northern component had disappeared (Fig. 9): the chlorophyll maximum fell to about 0.5 mg/m³, a concentration close to the mean value found at 40 or 50 m in similar conditions (Fig. 14).

The chlorophyll content in the 80 m upper layer ranged from 40 mg/m² (mean of 24 profiles from days 1 to 6) to 25 mg/m² (mean of 22 profiles from days 7 to 12). Primary production was also very high during the first 4 days, ranging from 1 to more than 2 gC/m²/day (Fukaï, 1991). Such values, typical of very productive areas, were not expected in poorly productive systems such as the convergence zone at 4°N. Similar rapid variations in both production and cur-

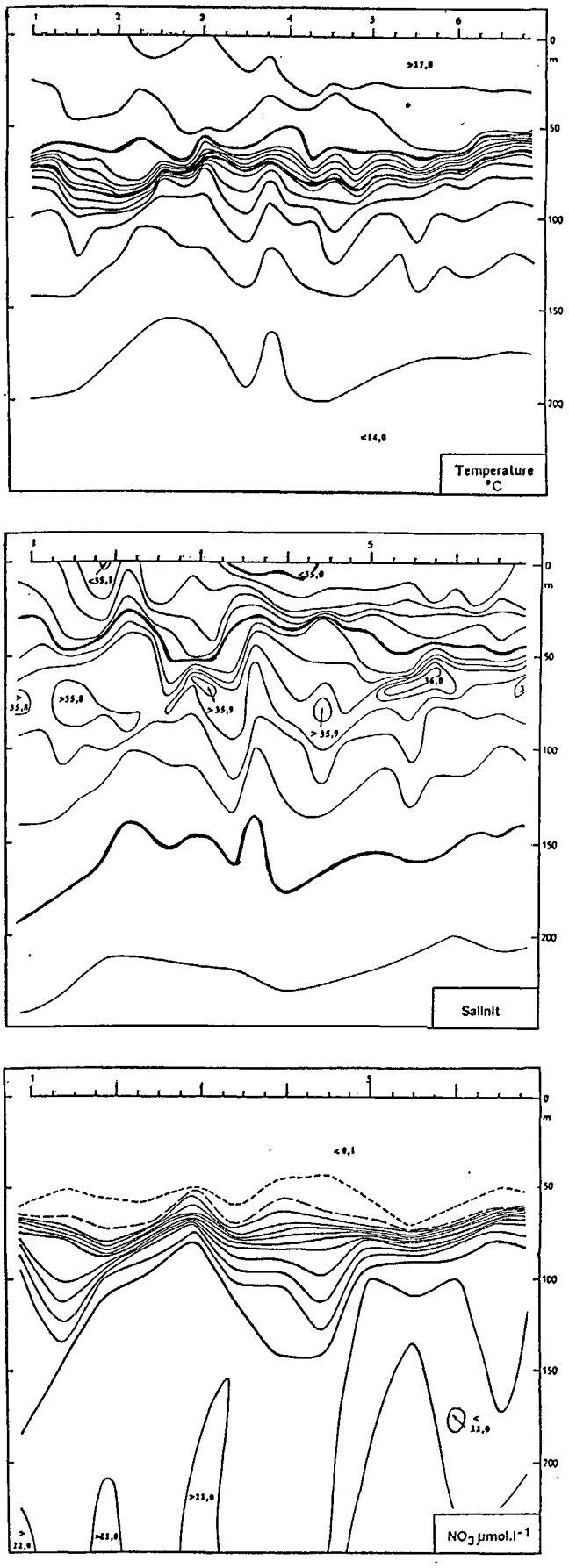

Figure 11

Vertical distribution of temperature (a), salinity (b) and nitrate (c) during the drift experiment of the PIRAL cruise in June 1986.

rent were previously observed at the equator (4°W) during a 14-day fixed position study (CIPREA cruise): the vertical hydrological stratification varied in response to the north-south oscillations of the equatorial current system. Chlorophyll and production were greatly influenced by these oscillations, as shown by a change in the primary production from 1 to 2 gC/m²/day within few days (Herbland and Le Bouteiller, 1982).

During the PIRAL cruise, nitrate, temperature and density were strongly correlated, as reported earlier in the Gulf of Guinea (Voituriez and Herbland, 1984). The chlorophyll maximum was systematically observed in waters showing the same range of nutrient, temperature and density. The isolines $NO_3 = 0.1$ and $NO_3 = 0.5$ mmol.m^{-3} corresponded to the mean densities 23.6 and 24.0 respectively. The thickness of the layer between the 23.6 and 24.0 isopycnes ranged from 40 to less than 2 m, indicating large changes of the vertical density gradient and mixing processes. All chlorophyll concentrations greater than 1 mg/m³ were associated with a weak nitrate gradient at the top of the nitracline and a weak vertical density gradient ($Ds/DZ < 0.05$). Conversely, when only few metres separated the two isopycnes, the top of the nitracline was enclosed within a strong pycnocline. Thus, mixing was reduced and nutrient input into the euphotic zone was minimal. In these conditions, the chlorophyll maximum concentration was observed around 0.5 mg/m³ (Fig. 15).

DISCUSSION AND CONCLUSIONS

In this paper we use a simulation based on a general circulation model of the Atlantic Ocean to describe long instability waves resulting from horizontal current shear. This description is in good agreement with earlier observations. During summer, organized undulations of the thermal front, associated with anti-cyclonic eddies, propagate westward along 3-4°N from 10 to 40°W through the equatorial Atlantic at a speed of around 30-40 km/day. The crests of the undulations are 900 to 1000 km apart, and the eddies have a longitudinal extension of 900 km and a latitudinal extension of 300 km. Annual and inter-annual signals exist for these propagations. Long instability waves do not exist throughout the year, so that the OGCM simulation does not generate long waves during March and April when the NECC vanishes. The simulation indicates the regular presence of long waves in autumn and early winter, though no temperature signature was visible at the surface. Some satellite observations during short cold events in boreal winter showed evidence of thermal front undulations similar to those associated with long wave propagations observed in summer. *In situ* observations during FGGE (Molinari *et al.*, 1983) confirm the existence of cold events in winter at the equator, and such events are well known along the Guinea Gulf coast.

The simulation clearly shows large vertical movements associated with anti-cyclonic eddies. In the eddies, upwelling and downwelling zones have a horizontal extension greater than 200 km, and vertical movements

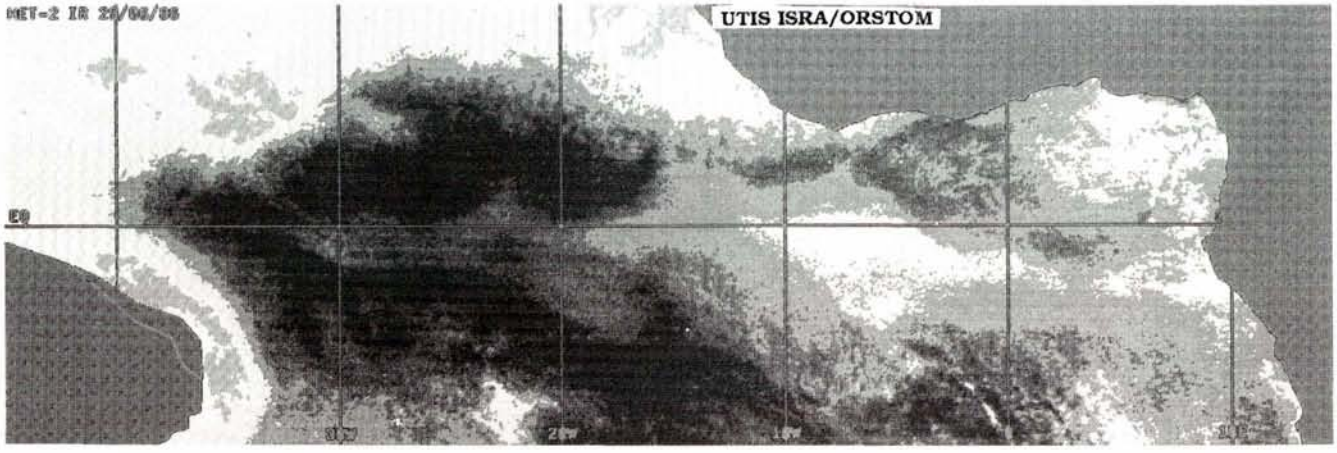

Figure 12

Image of SST in the equatorial Atlantic Ocean compiled from infrared METEOSAT data collected on 29 June 1986, confirming that long instability waves occurred during the PIRAL cruise.

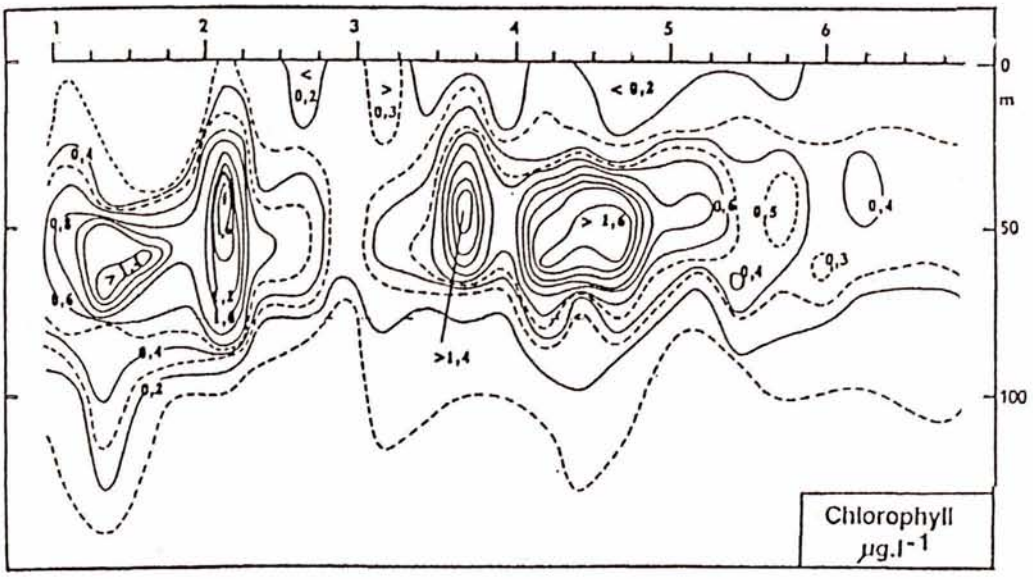

Figure 13

Vertical distribution of chlorophyll during the drift experiment of the PIRAL cruise in June 1986.

extend from the surface to 70 m in depth. Vertical velocities greater than 4 m/day are remarkable in comparison with the 1-2 m/day upward velocity in equatorial divergence computed by the simulation. Such vertical movements are likely to have an important biological impact. If they extend vertically throughout the thermocline, they can lift nutrients up into the euphotic layer and stimulate primary production. The thermocline (represented by the depth of the 20°C isotherm) is around 90 m at 4°N-30°W and around 55 m at 4°N-10°W (Fig. 16). Thus, the vertical movements associated with long instability waves could commonly reach the thermocline in the central part of the Atlantic basin (10-20°W). In this way, the long instability waves could affect biological production by "eddy pumping" around 4°N in the central part of the Atlantic Ocean. During the summer, the strong northward currents on the west side of the long wave anti-cyclonic eddies could transport high chlorophyll concentrations northward from the equatorial upwelling region. Thus, long instability waves could also play a role in affecting biological properties north of the equator by meridian advection.

The observed values during the PIRAL cruise are typical of very productive zones. The remarkably high chlorophyll concentrations (the highest values in our data bank for the equatorial Atlantic) and the high primary production values are associated with current movements similar to those in an anti-cyclonic eddy, which are characteristic of the long instability wave pattern. With speeds as high as those observed during the first days of the PIRAL cruise (140 cm/s), only a few days would be required for chlorophyll to be carried from the equator to 4°-5°N. The PIRAL data do not indicate whether the high chlorophyll concentrations observed at these latitudes result from eddy pumping

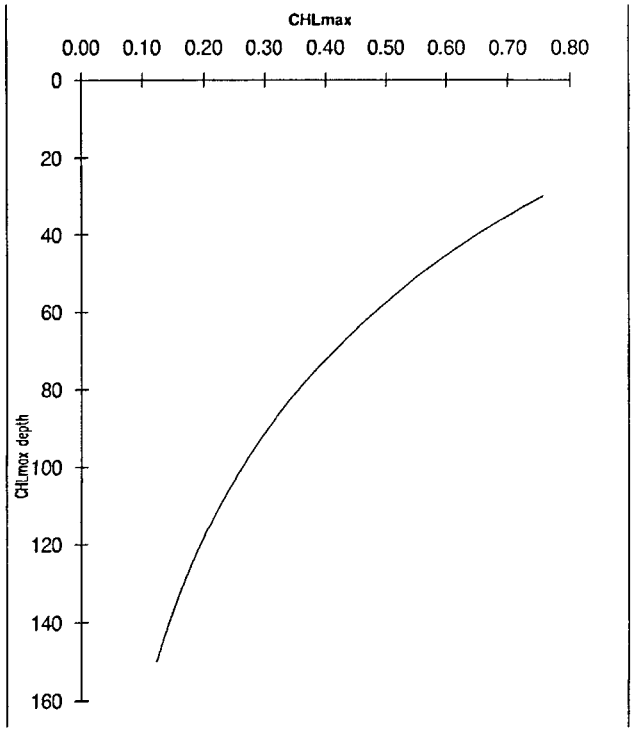

Figure 14

Mean deep chlorophyll maxima as a function of the depth of chlorophyll occurrence: from data collected since 1978 in the equatorial belt of the Atlantic Ocean from 20°N to 15°S, and from 35°W to 10°E (11 cruises, 546 profiles).

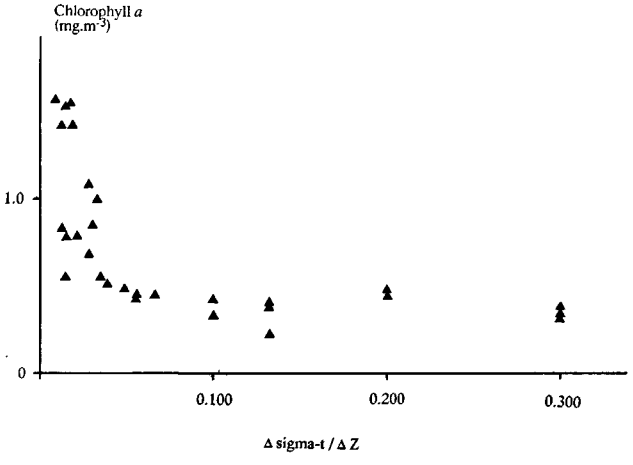

Figure 15

Relationship between chlorophyll maxima and the vertical density gradient during the drift experiment of the PIRAL cruise in June 1986.

(local upwelling due to instability dynamics) or from a vigorous meridian advection from the equatorial upwelling region. Certainly, both advection and eddy pumping are involved in the PIRAL values. In our opinion, these high chlorophyll concentrations are due to a combination of

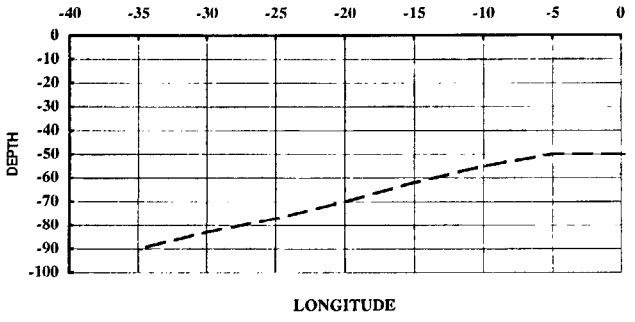

Figure 16

Mean thermocline depth (20 °C isotherm) along 4°N in the Atlantic (from TOGA XBT, J.P. Rebert, personal communication).

eddy pumping and meridian advection, but, such high concentrations have never previously been observed at this depth in the equatorial Atlantic. This leads us to believe that the local upwellings might play a major role. However, a complete set of observations is required to confirm and evaluate the respective role of each process linked to the tropical instability waves in the Atlantic ocean during the summer.

It is important to note the respective seasonal role of the two mechanisms involved. The meridian advection is biologically efficient, by transporting high chlorophyll concentrations from the equator northwards to around 4°N, only when the equatorial upwelling is well developed, *i.e.* during the summer season. In autumn and early winter, the tropical instability waves and the associated meridian advection still exist when the equatorial upwelling is no longer present, so during that period the biological impact of the meridian advection is certainly unimportant. Unlike the advection, the eddy pumping mechanism can be biologically active (where the thermocline is shallow enough), whenever the instability waves exist, *i.e.* during the summer, the autumn and the early winter. In summer, the high chlorophyll concentrations in the convergence zone may be explained by the two mechanisms. In autumn and early winter, the eddy pumping has to be considered alone as a possible productive process.

Each boreal autumn and early winter, large quantities of tuna are taken by purse-seiners (Fonteneau, 1993) in the area 2-5°N, 10-20°W. We suggest that the eddy pumping resulting from instability waves could account for the paradoxical situation of a very important tuna fishery located away from the typical productive zones of the tropical Atlantic (Voituriez and Herbland, 1982). This productive mechanism, active in small oceanic areas, could be very important for fisheries by yielding tuna concentrations during a period of the year when equatorial upwelling is absent but when the long instability waves still exist, and could account for the presence of tens of thousands of tunas during several months each year in the same area. Conversely, during equatorial upwelling in summer, biological production is spread out over the whole equatorial Atlantic and thus does not result in the concentrations of tuna so essential for purse-seine fisheries.

REFERENCES

Chartier M. (1985). Un modèle numérique tridimensionnel aux équations primitives de circulation générale de l'océan. Doctoral thesis, University Paris 6, France, 111 p.

Cox M.D. (1980). Generation and propagation of 30-day waves in a numerical model of the Pacific ocean. *J. Phys. Oceanogr.*, **10**, 1168-1186.

Düing W., Ph. Hisard, E. Katz, J. Meincke, L. Miller, K.V. Moroshkin, G. Philander, A.A. Ribnikov, K. Voigt and R.Weisberg (1975). Meanders and long waves in the equatorial Atlantic. *Nature*, **257**, 5524, 280-284.

Fonteneau A. (1993). La zone " Liberia ": quelques éléments statistiques et de réflexions halieutiques. IATTC Madrid, SCRS 93/112, 651-668.

Fukai E. (1991). Importance du picoplancton autotrophe dans la biomasse et la production primaire des eaux marines oligotrophes. Atlantique tropical oriental et mer des Sargasses. Doctoral thesis, University Paris 6, 150 p.

Hansen D.W. and C.A. Paul (1984). Genesis and effects of long waves in the equatorial Pacific. *J. Geophys. Res.*, **89**, 10431-10440.

Hellerman S. and M. Rosenstein, 1983. Normal monthly windstress over the world ocean with error estimates, *J. Phys. Oceanogr.*, **13**, 1093-1104.

Herbland A. and B. Voituriez (1979). Hydrological structure analysis for estimating the primary production in the tropical Atlantic ocean. *J. Mar. Res.*, **37**, 87-101.

Herbland A. and A. Le Bouteiller (1982). The meanders of equatorial currents. Influence on biological process. *Oceanogr. Trop.*, **17**, 15-25.

Hisard Ph., C. Hénin, R. Houghton, B. Piton and P. Rual (1986). Oceanic conditions in the Atlantic during 1983 and 1984. *Nature*, **322**, 243-245.

Large W.G. and S. Pond (1981). Open ocean momentum flux measurements in moderate to strong winds, *J. Phys. Oceanogr.*, **11**, 324-336.

Legeckis R. (1977). Long waves in the eastern equatorial Pacific; A view from a geostationary satellite, *Science*, **197**, 1177-1181.

Legeckis R. and G. Reverdin (1987). Long waves in the equatorial Atlantic ocean during 1983. *J. Geophys. Res.*, **92**, 2835-2842.

Legeckis R. and W. Pichel (1984). Monitoring of long waves in the eastern equatorial Pacific 1981-1983 using satellite multi-channel sea surface temperature charts. NOAA Tech. Rep. NESDIS 8, 19 p.

Legeckis R. (1986). Long waves in the equatorial Pacific and Atlantic oceans during 1983. *Ocean-Air Interactions*, **1**, 1-10.

Levitus S. (1982). Climatological atlas of the world ocean, NOAA prof. Paper 13, U.S. Govt. Printing Office, Washington D.C., 173 p.

Madec G., M. Chartier, P. Delecluse and M. Crépon (1991). A three-dimensional numerical study of deep water formation in the northwestern Mediterranean sea, *J. Phys. Oceanogr.*, **21**, 1349-1371.

Malardé J.P., P. de Mey, C. Périgaud and J.F. Minster (1987). The oceanic dynamic topography associated with Long equatorial waves. *J. Phys. Oceanogr.*, **17**, 2273-2279.

McPhaden M.J., M. Fieux and J. Gonella (1984). Meanders observed in surface currents and hydrography during an equatorial Atlantic transect. *Geophys. Res. Lett.*, **11**, 757-760.

Molinari R.L., E. Katz, E. Fahrbach, H.U. Lass and B. Voituriez (1983). Near surface temperature observations obtained in the equatorial Atlantic during FGGE (1979). In: Hydrodynamics of the equatorial ocean, Elsevier Oceanography Series 36. Ed. by J. Nihoul, Elsevier, p. 65-82.

Morlière A., P. Delecluse, P. Andrich and B. Camusat (1989a). Evaluation des champs thermiques simulés par un modèle de circulation générale de l'Atlantique tropical, *Oceanol. Acta*, **12**, 9-22.

Morlière A., G. Reverdin and J. Merle (1989b). Assimilation of temperature profiles in a general circulation model of the tropical Atlantic. *J. Phys. Oceanogr.*, **19**, 1892-1899.

Musman S. (1992). Geosat altimeter observations of long waves in the equatorial Atlantic. *J. Geophys. Res.*, **97**, 3573-3579.

Oudot C. (1987). Distributions verticales des propriétés physico-chimiques et de la biomasse végétale dans l'Atlantique tropical. FOCAL, vol. 2, Travaux et Documents ORSTOM, **209**, 215 p.

Oudot C. (1989). O2 and CO2 balance approach for estimating biological production in the mixed layer of the tropical Atlantic ocean (Guinea Dome area). *J. Mar. Res.*, **47**, 385-409.

Périgaud C. (1990). Sea level oscillations observed with Geosat along the two shear fronts of the Pacific North Equatorial Countercurrent. *J. Geophys. Res.*, **95**, 7239-7248.

Philander S.G.H. (1978). Forced oceanic waves. *Rev. Geophys.*, **16**, 15-46.

Philander S.G.H., W.J. Hurlin and R.C. Pacanowski (1986). Properties of long equatorial waves in models of the seasonal cycle in the tropical Atlantic and Pacific oceans, *J. Geophys. Res.*, **91**, 14207-14211.

Pullen P.E., R.L. Bernstein and D. Halpern (1987). Equatorial long wave characteristics determined from satellite sea surface temperature and in situ data. *J. Geophys. Res.*, **92**, 742-748.

Reverdin G., P. Delecluse, C. Levy, P. Andrich, A. Morlière and J.M. Verstraete (1991). The near surface tropical Atlantic in 1982-1984. Results from a numerical simulation and a data analysis. *Progress in Oceano.*, **27**, 273-340.

Richardson P.L. and G. Reverdin (1987). Seasonal cycle of velocity in the Atlantic north equatorial countercurrent as measured by surface drifters, current meters and ship drift, *J. Geophys. Res.*, **92**, 3691-3708.

Richardson P.L. and T.K. McKee (1984). Average variations of the Atlantic equatorial currents from historical ship drifts, *J. Phys. Oceanogr.*, **14**, 1226-1238.

Servain J., M. Seva, S. Lukas and G. Rougier (1987). Climatic atlas of the tropical Atlantic wind stress and sea surface temperature: 1980-1984, *Ocean-Air Interactions*, **1**, 109-182.

Steger J.M. and J.A. Carton (1991). Long waves and eddies in the tropical Atlantic ocean: 1984-1990. *J. Geophys. Res.*, **96**, 15 161-15 171.

Voituriez B. and A. Herbland (1982). Comparaison des systèmes productifs de l'Atlantique tropical est : dômes, upwelling côtier et upwelling équatorial. Rapp. et P.V. Cons. Explor. Mer, **180**, 107-123.

Voituriez B. and A. Herbland (1984). Signification de la relation nitrate/température dans l'upwelling équatorial du Golfe de Guinée. *Oceanol. Acta*, **7**, 169-174.

Weisberg R.H. (1984). Instability waves observed on the equator in the Atlantic ocean during 1983. *Geophys. Res. Lett.*, **11**, 753-756.